IV International Conference on Computational Methods for Coupled Problems in Science and Engineering
COUPLED PROBLEMS 2011
M. Papadrakakis, E. Oñate and B. Schrefler (Eds)

VORTEX-INDUCED VIBRATIONS OF AN ELASTICALLY MOUNTED CYLINDER WITH LOW MASS-RATIO AT RE=3900

YOANN JUS*, ELISABETH LONGATTE*, JEAN-CAMILLE CHASSAING† and PIERRE SAGAUT†

*LAMSID-UMR EDF/CEA/CNRS n° 2832
Clamart, France
e-mail: yoann.jus@gmail.com, elisabeth.longatte@edf.fr

†UPMC Univ Paris 06, UMR 7190, Institut Jean le Rond d'Alembert
F-75005 Paris, France

Key words: Fluid-structure Interaction, Vortex-Induced Vibrations

Abstract. The present paper deals with the numerical study of vortex-induced vibrations (VIV) of an elastically mounted cylinder in a cross flow with uniform inflow. It is well known that, in the case of low mass-damping, three distinct types of transverse amplitude response can be observed depending on the range of the reduced velocity. However, the accurate numerical simulation of the VIV amplitudes at the lock-in upper branch remains a great challenge. Moreover, few studies deal with the investigation of the hysteretic loop due to the jump between the initial excitation branch and the upper branch.

Here, we propose to compute the transverse motion of the structure at a Reynolds number equal to 3900 Large Eddy Simulation. The Navier-Stokes equations are solved on a moving and deforming grid by means of an Arbitrary Lagrangian Eulerian (ALE) co-located finite volume method for unstructured meshes. An iterative algorithm is used at each time step based on Newton's or fixed point method. This algorithm uses convergent explicit predictions of the coupled fluid structure system and sub-cycling is involved to get convergence towards the implicit solution of the fully coupled system. A criterion based on the structure velocity is used to stop the numerical sub-cycling process.

First, we compare the transverse amplitude response of the cylinder for various reduced velocities with the DNS results obtained by Lucor et al. (2005) for zero structural damping and a mass ration equal to 2. Next, the experimental data of Hover et al. (1998) are considered to demonstrate the ability of the present solver to predict the VIV response for low mass-damping.

1 INTRODUCTION

Solving multi-physics problems is still a challenge requiring advanced computational methods. This work aims to investigate flow-induced vibrations of dynamical systems subjected to

complex flows. In very confined areas such as those encountered in steam exchanger and heat generator tube arrays we are proposing a decomposition of physical problems by considering, as a first step, mechanical systems made of single cylinder subjected to cross-flows.

Typical response of tube array under cross-flow are described below. When there is no mean flow, this is the so-called region of Fluid Structure Interaction (FSI). Cylinders are subjected to two kinds of excitations : inertial effect on one hand, damping effect on the other hand. These effects are combined and generated by the presence of fluid inertia and viscosity impacting shear stress exerted on solid walls. They may largely depend on confinement and they act on vibratory response frequency and damping. In the presence of mean flow, flow patterns across cylinder array are very sensitive to cylinder arrangement as well as other parameters. Cylinder spacing is one of the most important geometric parameters. Conventional results propose a classification in flow regimes in standard in-line and staggered tube arrays. In several configurations, all cylinders shed Karman vortices but a jet swing associated with vortex shedding is also possible. Sometimes Karman vortices can not develop because the free shear layer of a front cylinder may become attached to the downstream cylinder. On the contrary, when the confinement decreases, vortex streets can be the same as those shed by isolated cylinders. There are several possible flow regimes and many studies have been performed to identify the borderlines between these flow regimes as flow regimes depend on all of the geometric and hydraulics parameters like Reynolds and Stokes numbers. There are three typical kinds of action exerted by fluid and flow on solid walls responsible for three different dynamical behaviours of tube array under cross flow : (1) Vortex-Induced Vibration (VIV) : in the lock-in frequency range, a synchronization occurs between vortex shedding frequency and solid response frequency, which implies an increase of displacement magnitude as well as a change of cylinder frequency. (2) Turbulence-Induced Vibration (TIV) : whenever the reduced velocity, cylinders are submitted to an external action exerted by fluid whose level is directly governed by the Reynolds number. The higher the Reynolds number value, the higher the level of turbulence and the associated loading which induces a moderate increase of vibration magnitude - without any change however in the dynamical stability regime of the cylinders. (3) Finally Motion-Induced Vibration (MIV) : when the reduced velocity reaches the critical threshold called the fluid-elastic instability threshold, vibration magnitude dramatically increases linearly and only non-linear effects like collision or breakdown can stop this motion.

The paper is organised as follows. A brief review of simulation of VIV are recalled in a first part. In the second part, numerical methods are described. The last section focuses on VIV and simulation of lock-in for a dynamic single cylinder under cross-flow.

2 STATE OF ART

Before dealing with multi-tube configurations (in-line or staggered tube arrays), single-cylinder configurations are investigated in this article. In the case of single cylinder, only the VIV phenomenon occurs. This phenomenon has been widely studied. So, it is well known that, in the case of an elastically mounted cylinder with low mass-damping, three distinct types of transverse amplitudes response can be observed. The distinction between the three response

branches arising in different ranges of the reduced velocity U^* has been described in the literature [13][14][15]. The reduced velocity U^* is defined by U_0/f_nD with U_0 the flow velocity, f_n the system natural frequency and D the cylinder diameter.

For low reduced velocities, there exists an *initial* branch associated with a 2S vortex shedding mode (two single vortices shed per cycle) and the mean forces and cylinder response are in phase. For intermediate and larger reduced velocities there is an *upper* and a *lower* branch associated with a 2P vortex shedding mode emission [13] [14] (two pairs of vortices shed per cycle). The 'lock-in' is characterized by a synchronization of the vortex shedding frequency (f_s) and the system natural frequency (f_n). The reduced frequency f^* is defined by the ratio between frequency of oscillation f_0 and f_n. At the lock-in, f^* tends to be equal to 1. At the 'lock-in', the reduced velocity U^* is directly related to the Strouhal number St. For a given reduced velocity, the amplitude of the response and the mode emission of the vortex shedding depend on the mass-damping parameter $m^*\xi$. m^* designates the mass ratio m/m_f with m_f the mass of displaced fluid for a single cylinder ($m_f = \rho\pi L_z D^2/4$) and ξ the reduced damping. However, very few numerical results have been able to accurately reproduce the three-branch response model obtained from experiments.

Reaching the *upper* branch response still remains a challenge. Hysteresis, three dimensional as well as low mass-damping effects have been highlighted in previous work (2D-FEM simulations of Singh and Mittal (2005) [16], 3D-DVM simulations of Yamamoto et *al.* (2004) [17] and 2D-FVM simulations of Placzek et *al.* (2007) [18]) but without the capture of the *upper* branch response of the cylinder. As the 'upper branch' regime is observed for moderate and high Reynolds numbers and therefore appears to be Reynolds-dependent. Al Jamal and Dalton (2004) [19] introduce turbulence modelling and perform 2D-LES simulations at $R_e = 8000$, without reaching the *upper* branch. However Guilmineau and Queutey (2004) [20] and Pan et *al.* (2007) [21] perform 2D-RANS simulations in a wide range of Reynolds numbers ($2000 < R_e < 10000$), which yield promising results, since the *upper* branch regime is observed by using an 'U^*-increasing' initial condition for simulations (i.e. by performing continuous simulations and gradually increasing the fluid upstream velocity - and the Reynolds number - while keeping all other parameters constant). However, the *upper* branch is not observed when using the 'from rest' conditions (i.e. setting the fluid upstream velocity at a given value and letting the cylinder freely oscillate under VIV). Recently, Sigrist et *al.* (2008) [22] yield the *upper* branch with a 2D RANS simulation but the extent of this higher amplitude zone is rather narrow when compared to the experiments. Vortex-Induced Vibrations involve complex three dimensional phenomena that can not be accurately simulated by using 2D modeling. Only Lucor et al. (2005) [23] obtain cylinder response results closely matching the 'three-branch response' mode proposed in experimental works. In particular, the existence of an *upper* branch with large amplitude response is confirmed by performing Direct Numerical Simulations (DNS) with low mass-damping (zero structural damping and mass ration $m^* = 2$) for Reynolds number range ($Re = 1000$ to 3000).

Numerical simulation of the turbulent wake of static and dynamic cylinders in cross flows is considered. Large Eddy Simulation (LES) is involved in the subcritical Reynolds number

range enabling large temporal spectra evaluations. A moving mesh formulation is used through an Arbitrary Lagrange Euler (ALE) method in order to deal with solid boundary motion and an iterative solver is used to account for fluid structure interfacial coupling. As far as fully-coupled fluid solid system computation is concerned, in the presence of strong non linearity of fluid, solid or interface dynamics (like turbulence or large magnitude motion), small perturbation development procedures relying on linearization of interfacial boundary conditions are prohibited. Therefore alternative methods involving iterative algorithms are prescribed. The present work proposes the resolution of a fully-coupled fluid solid system by using a staggered procedure suitable for non-matching interfaces. Thanks to a partitioned approach both fluid and solid subsystems are formulated, discretized and solved separately and an iterative algorithm is involved to ensure the convergence towards the solution ensuring energy transfer consistency through the interface.

3 NUMERICAL ASPECTS

Simulations presented in the framework of the present article rely on Navier-Stokes equation computations[1] by using a collocated finite volume method for unstructured meshes devoted to incompressible flows and turbulence with a fractional time step procedure for fluid pressure velocity coupled computation through a projection method [1].

The flow is assumed Newtonian with a constant density ρ. If $\underline{\overline{u}}$ and $\overline{p}$ stand for spatially filtered velocity and pressure, the filtered Navier-Stokes equations can be written as :

$$\frac{\partial \overline{u}_i}{\partial x_i} = 0 \tag{1a}$$

$$\frac{\partial \overline{u}_i}{\partial t} + \frac{\partial \overline{u}_i \overline{u}_j}{\partial x_j} = -\frac{1}{\rho}\frac{\partial \overline{p}}{\partial x_i} + \nu \frac{\partial^2 \overline{u}_i}{\partial x_j \partial x_j} - \frac{\partial \tau_{\mathrm{ij}}}{\partial x_j} \tag{1b}$$

with local coordinates (x, t) in the space time domain.

The subgrid scale tensor $\underline{\underline{\tau}}$ has to be modeled. The dynamic Smagorinsky model based on Germano identity and Lilly minimization is used [2] [3] to take into account the small structures that are mainly dissipative. The deviatoric part of the subgrid-scale tensor is given by :

$$\tau_{\mathrm{ij}} - \frac{1}{3}\tau_{\mathrm{kk}}\delta_{\mathrm{ij}} = -2\nu_t \overline{S}_{\mathrm{ij}} = -2(C_S\overline{\Delta})^2 \|S\| \overline{S}_{\mathrm{ij}} \tag{2}$$

where $\overline{S}_{\mathrm{ij}}$ represents the filtered strain rate tensor, $\|S\| = \sqrt{2\overline{S}_{\mathrm{ij}}\overline{S}_{\mathrm{ij}}}$, ν_t the subgrid-scale viscosity, $\overline{\Delta}$ the filter width and C_s the dynamic Smagorinsky constant. In this work all computational cells are hexahedral, therefore $\overline{\Delta} = 2\Omega^{\frac{1}{3}}$ can be used, where Ω is the volume of a computational cell. The term $\frac{1}{3}\tau_{\mathrm{kk}}\delta_{\mathrm{ij}}$ is taken into account in the pressure gradient. The filter which appears in equation (1) is implicit as it is introduced by the discretization errors in space

[1] With *Code_Saturne* (www.code-saturne.org) involving a SIMPLEC algorithm with a Rhie and Chow interpolation to avoid odd-even decoupling on structured meshes [1].

and time and by the model itself. The explicit filter which is applied to compute the dynamic constant C_s uses the neighbors sharing a node with the computational cell. No averaging in the homogeneous directions (the spanwise direction in theses cases) is performed. No negative value is allowed to the subgrid-scale viscosity and the maximum value of the dynamic constant is set to 0.065 (the standard Smagorinsky model value).

In the framework of collocated finite volume approach, all variables are located at the center of gravity of the cells. The momentum equations are solved by considering an explicit mass flux (the three components of velocity are thus uncoupled). A second order centred scheme in space and time is used. A Crank-Nicholson time scheme with a linearized convection and a second order Adams-Bashforth method for the part of the diffusion involving the transposed gradient operator, coupling velocity components are involved. A centred scheme is used for the convection operator. The non-orthogonalities are taken into account with an implicit reconstruction technique explained in [1]. When a non-orthogonal grid is used, the matrix contains only the orthogonal contributions of the different operators. The non-orthogonal part is added to the right hand side of the transport equation (thus, inner iterations are needed for the velocity and pressure equations to make the gradient reconstruction implicit). This approach is suitable for several academic cases (decaying isotropic turbulence, channel flow) and also for industrial ones (T-junctions, combustor chamber, tube arrays) [4][5].

Solving fluid solid coupled systems involves the resolution of fluid and solid dynamics simultaneously and in a coupled manner particularly at the interface where energy transfer takes place. Therefore a formulation of boundary conditions compatible with both fluid and solid systems is required. For a given interface, energy exchanges between fluid and solid domain occur through the interfaces of solid and fluid domains ($\Gamma_{s/f}$ and $\Gamma_{f/s}$). The energy transferred per unit of time and surface is defined by the product of mechanical stress acting on the interface and the interface displacement velocity. Therefore, the energy flux evaluated on each cell boundary located on fluid and solid interface models is consistent if at least two conditions are fulfilled in the continuum space : the continuity of the velocity and the stress at the interface. After space and time discretizations these conditions must be preserved with the required accuracy whatever the spacetime evolution of the boundaries. This implies an additional condition on the geometry continuity. At the interface :

$$\begin{cases} u_i = \dfrac{Du_i^s}{Dt} \ \text{ on } \ \Gamma_{f/s} \\ \sigma_{ij} n_j = T_{ij} n_j \ \text{ on } \ \Gamma_{s/f} \end{cases} \tag{3}$$

where u_s represents the displacement of the interface, $\frac{D}{Dt}$ the material derivative and T_{ij} the solid stress tensor. In this work, cylinder motion under crossflow is investigated. Considering small magnitude motion in the cross direction only if there is no degree-of-freedom of motion in the drag direction and assuming rigid body motion, the solid dynamic equation is expressed as follows :

$$m\,\ddot{y} + c\,\dot{y} + k\,y \;=\; F_y \tag{4}$$

where y is the transverse cylinder displacement, m the oscillating structural mass, c the structural damping, k the structural stiffness and F_y the action exercised by the fluid in the lift direction (small magnitude fluctuations around the mean equilibrium position). In the framework of rigid motion theory (similarly for linear elasticity), a lagrangian formulation is used to describe the time evolution of the solid kinematics. System remains linear and time integration relies on an implicit Newmark second order unconditionally stable algorithm.

In the fluid domain however standard Eulerian formulation is not suitable for describing solid boundary motion. Therefore an Arbitrary Lagrangian Eulerian (ALE) approach is involved. This moving grid method consists in introducing an arbitrary referential domain for Navier-Stokes system computation and using associated time-depending reference space mapping to derive the system to be solved in the computational coordinate system.

Thus, the governing equations in the ALE framework for an incompressible flow are written as follows :

$$\begin{aligned} &\rho\frac{\partial u_i}{\partial x_i} = 0 \\ &\frac{\partial u_i}{\partial t} + (u_i - v_i)\frac{\partial u_i}{\partial x_j} = -\frac{1}{\rho}\frac{\partial p}{\partial x_i} + \nu\frac{\partial^2 u_i}{\partial x_j \partial x_j} \end{aligned} \tag{5}$$

where v represents the cell velocity evaluated at the cell's center of gravity in a collocated finite volume approach. The introduction of an arbitrary computational reference system, from a mathematical point of view, means the introduction of a grid mesh impacting convective terms in the momentum equation. For incompressible flow, the Geometry Conservation Law (GCL) [6] is ensured for uniform flows with a first order approximation. It ensures numerical conservation of physical fields : the variation of an elementary volume during a time step Δt is balanced by the flux through the volume faces during the same period. The integral form of the GCL is :

$$\frac{\partial}{\partial t}\int_V dV = \int_{\delta V} w.ndS \tag{6}$$

Several formulations are possible to impose the grid velocity. In this work, a Poisson elliptic equation is introduced where variable $\overline{\overline{\lambda}}$ allows cell deformation [7] to be controlled :

$$\left\{ \begin{array}{rcll} \nabla \bullet (\overline{\overline{\lambda}}\nabla(v)) & = & 0 & \\ v & = & \dfrac{Du_s}{Dt} & \text{on } \Gamma_{f/s} \\ v & = & 0 & \text{on } \partial\Omega f \setminus \Gamma_{f/s} \end{array} \right. \tag{7}$$

The assumption that LES filtering commutes with partial derivatives is generally considered valid on fixed grids with uniform cell width. On deforming unstructured grid this is not the case anymore and temporal commutation errors (TCE) may have to be considered. In this work, the TCE are neglected in a first approximation. Finally to deal with computation of the fully-coupled fluid solid system, an iterative method is involved in order to look for a solution ensuring continuity conditions through the interface at each step of the calculation [7][8][9][10][11].

A fixed point method is used with consistent predictor and corrector terms for kinematics and stress field transfer associated with a projection and a condensation method in order to enable one-degree-of-freedom systems for modeling solid dynamics [12]. Under-relaxation may be introduced to improve the convergence properties of the iterative scheme.

4 NUMERICAL RESULTS AND DISCUSSION

A single cylinder motion under crossflow is studied. This is a first step before investigating cylinder arrangements in the future. The main objective of this part is to investigate numerically the behavior of a rigid cylinder at low mass-damping parameter, constrained to oscillate transversely to a free stream. The *upper* branch is particularly considered.

Numerical calculations are performed for two configurations : with and without damping. The experimental work of Hover et al. (1998) [24] and numerical results of Lucor et al. [23] are taken respectively as experimental and numerical references. Simulations are performed in a range of reduced velocities which extends from $U^* = 2$ to $U^* = 10$ for the case with damping and for $U^* = 5, 6, 7$ for the case without damping. Response of the cylinder undergoing VIV is analyzer in terms of amplitude and frequency of oscillations.

Before presenting results, some numerical parameters need to be specified. The size of the computational domain is $20D \times 20D \times 4D$. The length of the computational domain upstream the cylidner is equal to $10D$. This is necessary to allow the pressure field to reach an upstream asymptotic behaviour. A mesh with 32 points in the transversal direction is used and the total number of cells is equal to 2.10^6. Constant boundary conditions are introduced at the inlet (constant velocity in space and time) and no syntetic method is involved to generate turbulence. The flow is laminar upstream of the cylinder. No wall functions have been necessary during the unsteady simulations. Periodic boundary conditions are used in the spanwise direction. The outlet conditions are standard, Dirichlet condition for the pressure and homogeneous Neumann codition for the velocity. Symmetry boundary conditions are used for the upper and lower boudary faces. At the moving boundary, a Dirichlet condition is imposed for velocity with respect to the kinematic consistency condition. The Reynolds number $R_e = 3900$ has been used. The maximum CFL number is equal to 0.8. The corresponding time step is $\Delta t = 0.001D/U_0$ where U_0 is the inlet velocity. Initial conditions for the flow field are set by a static computation.

4.1 Case without damping

In a first case, we set the structural damping to be zero as we are interested in the maximum response of the system. The choice of mass ratio ($m^* = 2$) and structural damping corresponds to a low mass-damping parameter range. The parameters are the same as the numerical references [23]. We investigate three different reduced velocities $U^* = 5, 6, 7$ for the oscillator, see table 1. All the cases corresponds to the upper branch region.

A_{mean} corresponds to the mean amplitude averaged on 10 oscillation periods, A_{max} to the maximum amplitude and A_{min} to the minimum amplitude computed. The deviation corresponds to the standard deviation from the mean amplitude A_{mean}.

m^*	$m^*\xi$	V_r	A_{mean}/D	A_{max}/D	A_{min}/D	Deviation
2	0	5	0.795	0.909	0.579	0.096
2	0	6	0.694	0.836	0.632	0.062
2	0	7	0.532	0.593	0.441	0.043

Table 1: Average, maximum, minimum amplitude of response and deviation versus reduced velocity without damping

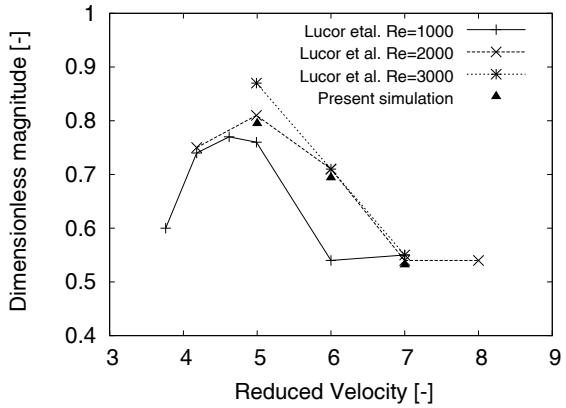

Figure 1: Dimensionless displacement at Reynolds 3900 at mass ratio $m^* = 2$ without damping versus reduced velocity with comparison to numerical [23] references

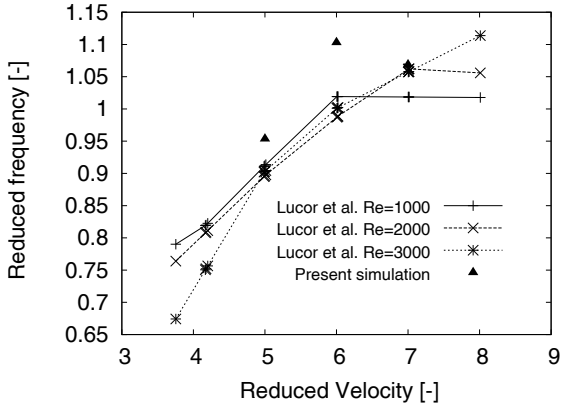

Figure 2: Evolution of reduced frequency at Reynolds 3900 at mass ratio $m^* = 2$ without damping (right) versus reduced velocity with comparison to numerical [23] references

As illustrated by the figure 1, the amplitude response of *upper* branch is Reynolds-dependent. For $U^* = 5$, amplitude response is lower than DNS results at Reynolds number 3000 and similar for other reduced velocity values ($U^* = 6, 7$). The first reason is clearly due to the difference of turbulence modelling and a second explanation can be the number of points along the spanwise direction (LES simulations were performed using 32 points whereas DNS simulations used 64 points).

Figure 4.1 gives the evolution of the frequency ratio f^* of the cylinder oscillations throughout the reduced velocity. The numerical results correlate well with the 'lock-in' zone except the reduced frequency for $U^* = 6$ is much larger than the numerical reference [23] for lower Reynolds number.

The simulation results are satisfactorily when compared to DNS results at least from a CPU cost point of view. This approach will be compared to an experimental reference : a cylinder with structural damping.

4.2 Case with damping

Numerical calculations are performed at low mass ratio ($m^* = 1$) and low mass-damping ($m^*\xi = 0.04$), which corresponds to the conditions of experimental references [24].

We present amplitude response results for $Re = 3900$ and investigate 8 cases for the oscillator with damping (table 2). A_{mean} gives the mean amplitude averaged on 10 oscillation periods, A_{max} the maximum amplitude and A_{min} the minimum amplitude computed throughout the reduced velocity range $2 < U^* < 10$. The deviation corresponds to the standard deviation from the mean amplitude A_{mean}.

For the case with damping, good correlations are observed as far as the *upper* branch is concerned. The highest average of the mean magnitude response of the cylinder around $A_{mean} \sim 0.795$ is obtained for a reduced velocity about $U^* = 5$. The extent of this higher amplitude zone correlates with the experimental data.

m^*	$m^*\xi$	V_r	A_{mean}/D	A_{max}/D	A_{min}/D	Deviation
1	0.04	2	0.081	0.121	0.052	0.019
1	0.04	3	0.380	0.416	0.352	0.33
1	0.04	4	0.794	0.892	0.663	0.052
1	0.04	5	0.795	1.01	0.639	0.056
1	0.04	5.5	0.721	0.898	0.562	0.107
1	0.04	6	0.715	1.08	0.547	0.149
1	0.04	7	0.661	0.821	0.550	0.072
1	0.04	10	0.488	0.546	0.413	0.045

Table 2: Average, maximum, minimum amplitude of response and deviation versus reduced velocity with damping

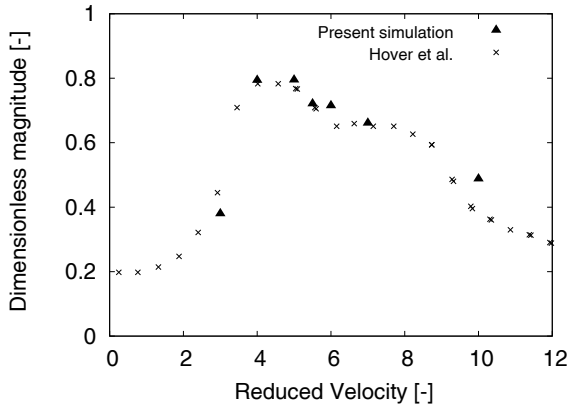

Figure 3: Dimensionless displacement at Reynolds 3900 at mass ratio $m^* = 1$ and damping ($m^*\xi = 0.04$) versus reduced velocity with comparison to experimental [24]

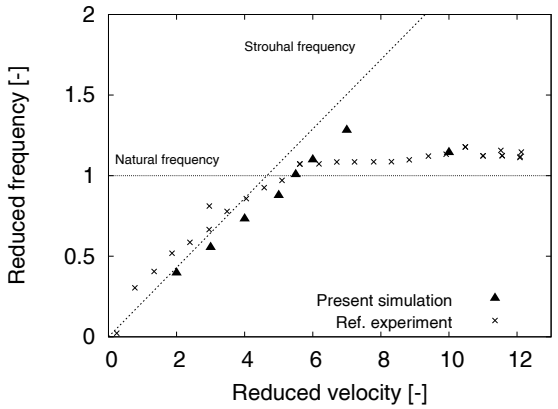

Figure 4: Evolution of reduced frequency at Reynolds 3900 at mass ratio $m^* = 1$ and damping ($m^*\xi = 0.04$) versus reduced velocity with comparison to experimental [24] references

Figure 4.2 gives the evolution of the frequency ratio f^* of the cylinder oscillations throughout the reduced velocity. The numerical results correlate well with the 'lock-in' zone.

The different branches of amplitude response are very well characterized by plotting not only the amplitude, but also the phase ϕ between the lift force and displacement, and the Lissajou figures or phase plane portraits of lift versus displacements (figure 5).

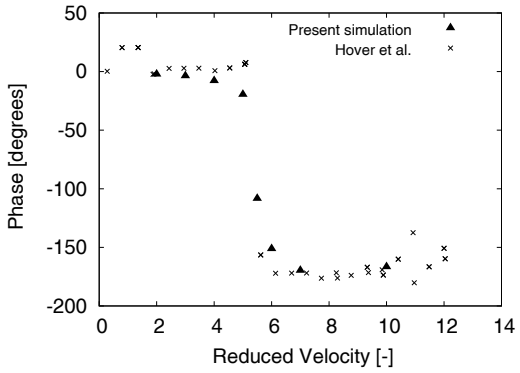

Figure 5: Phase between the lift force fluctuations and the displacement at Reynolds 3900 at mass ratio $m^* = 1$ and mass-damping ($m^*\xi = 0.04$) as a function of reduced velocity with comparison to experimental work [24]

The phase delay is evaluated by computation of cross power spectral density. The jump in phase angle ϕ in this figure is associated with the transition from the *upper* to the *lower* branch. If the phase ϕ is defined as the lead of the lift force fluctuations over the displacement, then the *upper* is near $0°$, whereas the *lower* branch is nearer $180\,°$, such as that found for a linear forced system going through resonance. When the dynamics shifts from the *initial* to the *upper* branch, the phase angle ϕ remains at just above $O\,°$. The Lissajou figures indicate the very periodic nature of the oscillations in the *lower* branch (figure 6 left) and the relatively less steady dynamics of the *upper* branch (figure 6 right). In the latter case, shown by the Lissajou on figure 7 left, the phase changes of around $180\,°$ as the oscillations seem to wander to the smaller amplitude of the *lower* branch, and then back by $-180\,°$ as the oscillations switch back to the larger amplitude of the *upper* branch. There is an intermittent switching between the *upper* and *lower* branch amplitudes and phases, whereas we see a hysteretic change from the *initial* to the *upper* branch. The phase portraits (figures 6, 7) can be compared to those plotted by [13] (see figure 13 in this reference).

The maximum lift (r.m.s.) occurs (figure 8) at the transition between the initial excitation and the *upper* branch. It is indeed very low in *lower* branch. As Khalak and Williamson (1999) [13], the lift increases rapidly brefore the transition and decreases after the transition.

The presented simulations yield the *upper* branch response which has never been reported so far with a 3D LES approach. The simulation results are therefore satisfactorily when compared to DNS results at least from a CPU cost point of view, since this approach can be considered

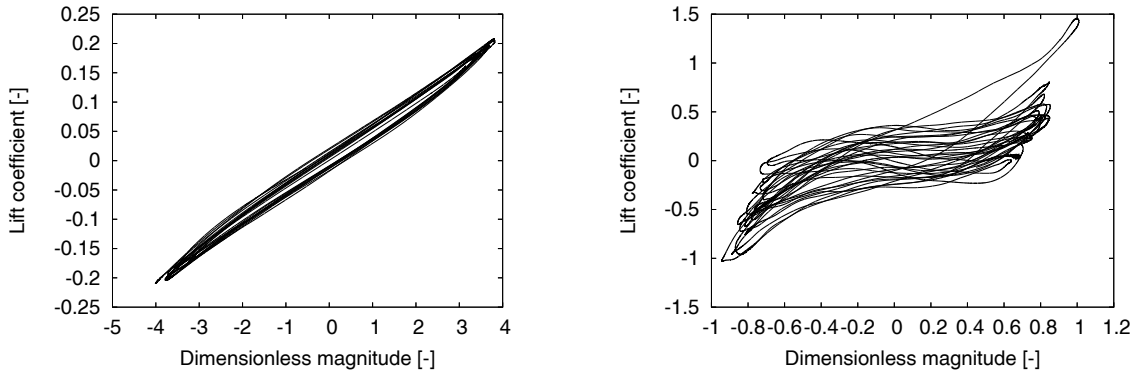

Figure 6: Phase plane for $U^* = 3$ (left) and $U^* = 5$ (right) at mass ratio $m^* = 1$ and damping ($m^*\xi = 0.04$)

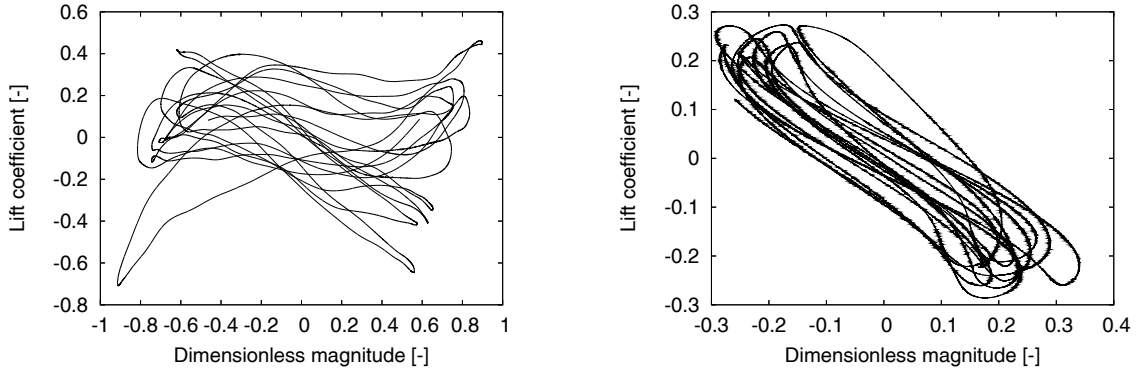

Figure 7: Phase plane for $U^* = 5.5$ (left) and $U^* = 10$ (right) at mass ratio $m^* = 1$ and damping ($m^*\xi = 0.04$)

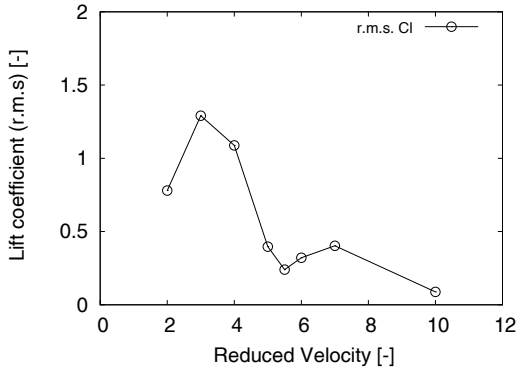

Figure 8: Variation of lift force coefficient versus reduced velocity for $m^* = 1$ and $m^*\xi = 0.04$

for practical applications. Further investigations will be devoted to the transitions between the branches.

5 CONCLUSIONS

Numerical simulations of the VIV response of a cylinder freely vibrating transversely to a fluid flow at moderate Reynolds number has been performed in the present study under low mass-damping conditions. Simulations are performed by using a coupled CFD/CSM procedure, with a single degree-of-freedom solid system and LES for modeling turbulent flow. Numerical results have been exposed and compared with experiments of Hover et al. (1998) on the one hand and simulations of Lucor et al. (2005) on the other hand. The presented simulations yield the *upper* branch response which has never been reported so far with a 3D LES approach. The simulation results are therefore satisfactorily when compared to DNS results at least from a CPU cost point of view, since this approach can be considered for practical applications. Qualitative agreements are highlighted as far as the cylinder response oscillation amplitude and frequency is concerned. Furthermore, the presented numerical simulations yield the *upper* branch response which has never been reported so far in CFD computations. Further investigations will be devoted to the transitions between the branches.

REFERENCES

[1] F. Archambeau, N. Méchitoua, M. Sakiz, *A finite volume code for the computation of turbulent incompressible flows - industrial applications*, International Journal of Finite Volumes, 1, 2004.

[2] M. Germano, U. Piomelli, P. Moin, W. Cabot, *A dynamic subgrid-scale eddy viscosity model*, Physics of Fluids, 3(7), 1760-1765, 1991.

[3] D. Lilly, *A proposed modification of the germano subgrid-scale closure method*, Physics of Fluids, 4, 633-635, 1992.

[4] S. Benhamadouche, *Large eddy simulation with the unstructured colocated arrangement*, Ph.D. thesis, Manchester University, 2006.

[5] S. Benhamadouche, D. Laurence, *LES, coarse LES, and transient RANS comparisons on the flow across tube bundle*, International Journal Heat and Fluid Flow, 4, 470-479, 2003.

[6] M. Lesoinne, C. Farhat, *A geometric conservation for flow problems with moving boundaries and deformable meshes, and their impact on aeroelastic computations*, Computer Methods in Applied Mechanics and Engineering, 134, 71-90, 1996.

[7] F. Huvelin, Couplage de codes en interaction fluide-structure et applications aux instabilités fluide-élastiques, PhD thesis, 2008.

[8] E. Longatte, V. Verreman, M.Souli, *Time marching for simulation of fluid structure interaction problems,* Journal of Fluids and Structures, 25, 95-111, 2009.

[9] S. Piperno, *Explicit/implicit fluid/structure staggered procedure with a structural predictor and fluid subcycling for 2D inviscid aeroelastic simulations,* International Journal of Numerical Methods In Fluids, 25, 1207-1226, 1997.

[10] S. Piperno, C. Farhat, *Partitionned procedures for the transient solution of coupled aeroelastic problems,* Computer Methods in Applied Mechanical and Engineering, 190, 3147-3170, 2001.

[11] M. Schaefer, M. Heck, S. Yigit *An Implicit Partitioned Method for the Numerical Method of Fluid-Structure Interaction,* p. 171-194, H.-J. Bungartz and M. Schäfer, editors, Fluid-Structure Interaction, LNCSE 53, Springer, 2007.

[12] N. Maman, C. Farhat, *Matching fluid and structure meshes for aero-elastic computations : a parallel approach,* Computers & Structures, 54 (4), 779-785, 1995.

[13] A. Khalak, C.H.K. Williamson, *Motions, Forces and Mode Transitions in Vortex-Induced Vibrations at Low Mass Damping,* Journal of Fluids and Structures, 13, 813-851, 1999.

[14] R. Govardhan, C.H.K Williamson, *Modes of Vortex Formation and Frequency Response of a Freely Vibrating cylinder,* Journal of Fluid Mechanics, 420, 85-130, 2000.

[15] C.H.K. Williamson, R. Govardhan, *Vortex-induced vibrations,* Annual Review of Fluid Mechanics, 36, 413-455, 2004.

[16] S.P. Singh, S. Mittal, *Vortex-Induced Vibration at Low Reynolds Numbers : Hysteresis and Vortex-Shedding modes,* Journal of Fluids and Structures, 20, 1085-1104, 2005.

[17] C.T. Yamamoto, J.R. Meneghini, F. Saltara, R.A. Fregonesi, J.A. Ferrari, *Numerical Simulation of Vortex-Induced Vibration on Flexible Cylinders,* Journal of Fluids and Structures, 19, 467-489, 2004.

[18] A. Placzek, J.F. Sigrist, A. Hamdouni, *Numerical Simulation of Vortex Shedding Past a Circular Cylinder at Low Reynolds Number with Finite Volume Technique. Part II : Flow Induced Vibrations.,* Pressure Vessel and Piping, San Antonio, 22-26 July 2007.

[19] H. Al-Jamal, C. Dalton, *Vortex Induced Vibrations Using Large Eddy Simulation at a Moderate Reynolds number* Journal of Fluids and Structures, 19, 73-92, 2004.

[20] E. Guilmineau, P. Queutey, *Numerical Simulation of Vortex-Induced Vibration of a circular cylinder with Low Mass-Damping in a Turbulent Flow,* Journal of Fluids and Structures, 19, 449-466, 2004.

[21] Z.Y. Pan, W.C. Cui, Q.M. Miao, *Numerical Simulation of Vortex-Induced Vibration of a Circular Cylinder at Low mass-damping Using RANS Code,* Journal of Fluids and Structures, 23, 23-37, 2007.

[22] JF. Sigrist, C. Allery, C. Beghein, *A Numerical Simulation of Vortex Induced Vibrations on a Elastically Mounted Circular rigid Cylinder at Moderate Reynolds Numbers,* Pressure Vessel and Piping, Chicago, 27-31 July 2008.

[23] D. Lucor, J. Foo, G.E. Karniadakis, *Vortex mode selection of a rigid cylinder subject to VIV at low mass damping,* Journal of Fluids and Structures,20, 483-503, 2005.

[24] F.S Hover, A.H. Techet, M.S. Triantafyllou, *Forces on oscillating uniform and tapered cylinders in crossflow,* Journal of Fluid Mechanics, 363, 97-114, 1998.